This project has received funding from the European Union's Horizon 2020 research and innovation programme under Grant Agreement No 871106

Deliverable Number: D9.4	**Due date: 30 June 2024**
Deliverable Title: Magnet pre-designs for the roadmap **WP number: WP 9** **Leader Beneficiary: CNRS** **Deliverable type: Report** **Dissemination level: Public**	Reporting period: M6-M44 Issue date: 08 July 2024 Authors: Jérôme BEARD (CNRS), Christophe TROPHIME (CNRS), Frans WIJNEN (RU), Sergei ZHERLITSYN (HZDR) Reviewers: Oliver PORTUGALL (CNRS), Michel SEGRETI (CEA), Sylvain ROUX (CEA), ISABEL Board Status: Submitted

ISABEL

Improving the sustainability of the European Magnetic Field Laboratory

MAGNET PRE-DESIGNS FOR THE ROADMAP

Start date of the project: 1st November 2020

Duration: 60 months (48 months + 12 months by Amendment)

Project Coordinator: Geert Rikken – CNRS LNCMI (P1 - CNRS)

Contact: isabel@lncmi.cnrs.fr

Version	Modifications	Date	Authors
1.0	First draft	4 June 2024	See header
2.0	Final version	26 June 2024	See header
2.1	Corrected version	4 July	ISABEL Board
3.0	New Final version	5 July	See header
4.0	New Final version	8 July	See header

This project has received funding from the European Union's Horizon 2020 research and innovation programme under Grant Agreement No 871106

TABLE OF CONTENTS

This project has received funding from the European Union's Horizon 2020 research and innovation programme under Grant Agreement No 871106

1 Introduction

In this document we grouped two pre-design studies serving as deliverables. The first pre-design deals with Bitter magnets and the second one concerns non-destructive pulsed magnets targeting 110 T and beyond at the EMFL.

2 Pre-design studies

2.1 Pre-design studies on Bitter magnets

2.1.1 Introduction

This report provides an overview of the pre-design studies on Bitter magnets. The goal is to improve the Bitter magnets of the Laboratoire National des Champs Magnétiques Intenses (LNCMI), the French magnetic field facility, which is operating DC high-field resistive magnets in Grenoble up to 37 tesla. The actual Bitter magnets are designed for a 12 MW power installation. The study targets the design of Bitter magnets for an 18 MW power installation, which is in operation at LNCMI since September 2023. The new Bitter magnets must have the same dimensions than the actual ones. The only difference is the number of disks composing the Bitter Magnet and the stacking scheme.

We, also, present a joint effort on the modelling of these magnets. This work is the result of our discussions on the Magnet Design Center for resistive magnets. We identify the need for a 2D axially symmetric numerical finite element model (FEM) for the resistive magnets to complement the existing tools. Besides, we also initiate some comparisons and benchmarking of our respective tools.

The report starts by a presentation of this joint modelling effort. The design studies are then described. The target are Bitter magnets of the LNCMI: namely composed of an "inner" and "outer" coil. We consider separately the design of the two coils. Finally, we explore the implementation costs of the proposed new Bitter magnets.

This project has received funding from the European Union's Horizon 2020 research and innovation programme under Grant Agreement No 871106

2.1.2 Joint effort for Bitter magnet modelling

This section describes the work done on the modelling of Bitter magnets and the design tools developed at the LNCMI in Grenoble and the HFML in Nijmegen.

A Bitter magnet is a stack of copper-alloy disks with cooling slits. The disks also have larger holes to accommodate tie-rods, used to align the disks and fixate the stack. Segments of a suitable insulator, such as Kapton, are placed at regular angle to shape a helical current path in the stacking. This complex structure explains why we need to revert to simpler "geometries" to numerically model Bitter magnets. A common approach consists in considering first a 2D axisymmetric view of the Bitter magnet to get estimates for the magnetic field B and temperature T within the magnet. Analytical expressions are used at this step assuming a constant electrical resistivity ρ in the Bitter disks. Then, 2D simulations on a sector of a Bitter disk in the section where the magnetic field is the highest are made to obtain better insights of the temperature and stress $\bar{\bar{\sigma}}$ profile. In this work, we implement a FEM fully coupled model to re-consider the Bitter 2D axially symmetric simulation considering the dependence of ρ on T: $\rho=\rho_0\,(1+\alpha\,(T-T_0))$, with T_0 a reference temperature, ρ_0 the resistivity at T_0 and α the temperature resistance coefficient.

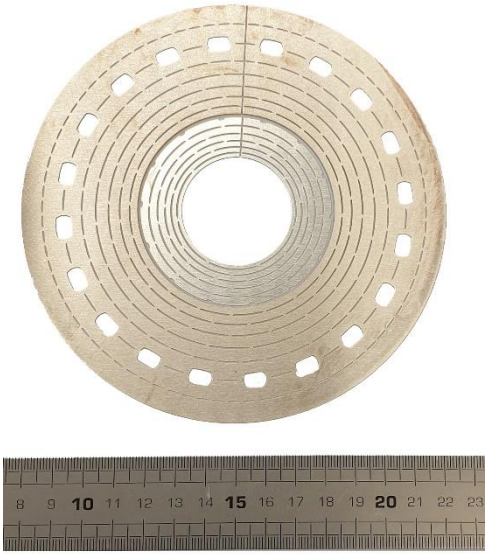

Figure 2.1.1: Bitter disks from HFML 38 T innermost coils: "big" holes correspond to tie-rods that will hold all the plates together, "small" holes are the cooling slits that cool the heat produced by Joule losses.

The model relies on the following system of partial differential equations (PDEs):

$$\boldsymbol{\nabla}\times\left(\frac{1}{\mu}\boldsymbol{\nabla}\times\vec{\boldsymbol{A}}\right)=\vec{\boldsymbol{J}}$$

$$-\boldsymbol{\nabla}\cdot(k\boldsymbol{\nabla}T)=-\frac{1}{\rho}\vec{\boldsymbol{J}}\cdot\vec{\boldsymbol{J}}$$

$$-\boldsymbol{\nabla}\cdot\bar{\bar{\sigma}}=\vec{\boldsymbol{J}}\times\vec{\boldsymbol{B}}$$

with $\vec{\boldsymbol{J}}=-1/\rho\boldsymbol{\nabla}V$ the current density. V is the solution of the Laplace equation with Dirichlet boundary condition for the input and output current. $\boldsymbol{A}$ is the magnetic vector potential defined as:

$$\vec{\boldsymbol{B}}=\boldsymbol{\nabla}\times\vec{\boldsymbol{A}}\ \text{ with }\ \boldsymbol{\nabla}\cdot\vec{\boldsymbol{A}}=0$$

From the first of the three PDEs, we can show that B can also be obtained by the Biot-Savart law:

$$\vec{B}(X)=\int_{\Omega}\frac{\partial G(X,Y)}{\partial\vec{n}_Y}\times\vec{J}(Y)d\Omega_Y$$

This project has received funding from the European Union's Horizon 2020 research and innovation programme under Grant Agreement No 871106

where $G(X,Y)$ and Ω denote, respectively, the Green Kernel and the Bitter geometry.

In 2D axisymmetrical geometries, $\boldsymbol{A}$ and $\boldsymbol{J}$ have only an azimuthal component. Note that, by construction in this case, $\boldsymbol{A}$ satisfies the Coulomb gauge. The electrical potential V simply reads as $U/(2\pi)$ with U the applied difference in potential on a turn.

The Bitter water cooling is modeled using Robin-type boundary conditions on each cooling slits:

$$-k\frac{\partial T}{\partial \mathbf{n}} = h(T - T_w),$$

with h the heat-exchange coefficient, T_w the water temperature and n the exterior normal to the boundary. The heat exchange coefficient for each cooling slit is obtained by standard correlations. In this study, we mostly use the heuristic correlation proposed by B. Montgomery, which states:

$$h = 1426.4\left(1 + 1.5\cdot 10^{-2}(T_w - 273)\right)\frac{\langle v_w\rangle^{0.8}}{d_H^{0.2}}$$

where $\langle v_w\rangle$ is the average water speed in the cooling slits, and d_H is the hydraulic diameter of the slits. Let $\sum S_w$ denote the total area of the cooling slits in a Bitter disk. As the water flow rate $Q=\langle v_w\rangle\cdot\sum S_w$ is controlled by the magnet input current (I) at the LNCMI-G installation, h depends on the solution of the PDEs. Namely, h is a function of $I = \int_S \vec{J}\cdot\hat{n}dS$. The water temperature rise, ΔT_w, in the magnet is derived from an energy balance:

$$\Delta T_w = \frac{P}{\rho_w C_p Q},$$

with P the total electric power dissipated in the Bitter magnet. T_w, along the magnet height, would vary from an input value T_{ini} up to $T_{ini}+\Delta T_w$. In our mode, T_w is assumed to be constant and equal to $T_{ini}+\Delta T_w/2$. Again, by construction T_w is a function of T_{ini} and I. Note that more realistic values have also been considered: the same procedure can be used to define the water-temperature rise per cooling slits provided that we can estimate the power P dissipated in the cooling slits. This can be done when post-processing the results.

If we assume that ρ is constant, we can derive analytical expressions for $\boldsymbol{J}$, $\boldsymbol{B}$ (using Biot-Savart) and T. These expressions are used by HFML in-house code to provide quick estimates for rapid design. To account for the magnet cooling, it is possible to use an iterative procedure using $\rho(\langle T\rangle)$ for each iteration. To get more insight, numerical simulations are carried out.

In this paper, we consider a numerical model for the 2D axial geometry with $\rho(T)$. The only assumption, here, is that the cooling slits are replaced by equivalent cooling rings – that is, with the same d_H. To solve the system of PDEs, we actually use an iterative procedure starting with an initial guess U (i.e. U_s per section of the considered Bitter magnet) to get $h(I)$, $\Delta T_w(I)$. After each iteration, U is updated such that the current in each Bitter section corresponds to the nominal current I_o times n_s the number of turns of the considered section. Indeed, in the 2D axial assumption, the current in a Bitter section is:

$$I_s = n_s I_o = \int_S -\frac{U_s}{\rho 2\pi r} dS$$

In a first step, we used the 1D HFML model to estimate the temperature profile along the radius in the midplane of the new inner Bitter coil. In this model, the geometry is supposed to be axisymmetric. The cooling holes are represented by equivalent cooling rings with the same cooling surface and the same hydraulic diameter as a single hole. Note that in this model, we also consider that there is some water flow in the tie-rod holes. The heat-exchange coefficient for each cooling surface is given by the Montgomery correlation. As for the water flow, the water velocity is derived from an expression involving the pressure losses in the cooling holes and the friction factor *f*. This friction factor is classically estimated with the Coole-Brooke equation with an average roughness of 0.025 mm. In the LNCMI 2D axial model, the magnet cooling is modeled following the same assumptions, but no cooling is assumed in the tie-rod holes. Comparisons of computed temperature distribution along *r* at position *z* = 0 is plotted on Figure 2.1.2. We clearly see the impact of the no cooling assumption on the tie-rods (near *r* = 300mm) in the LNCMI model. The difference between the two models arises from the heat exchange at the cooling slits. Indeed, in the LNCMI model, we have introduced a "filling factor" for each cooling "ring" that represents the ratio between the actual cooling slits wetted perimeter and the corresponding cooling rings wetted perimeter. This "filling factor" reduces the heat exchange on the rings, leading to a higher temperature in the Bitter magnet.

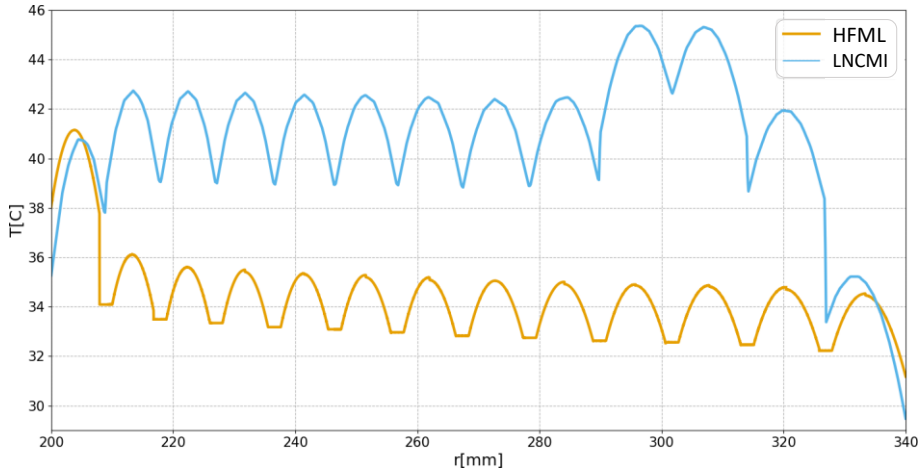

Figure 2.1.2: Temperature profile vs radial position at z=0 mm for I=31 kA.

In a second step, we consider 2D models of the Bitter magnets in the midplane (aka z = 0) to have more realistic estimates of the temperature distribution and, more importantly, of the stress distribution. For this purpose, we use HFML tools. Computed distributions of *T* and von Mises $\bar{\bar{\sigma}}$ are respectively displayed in Figure 2.1.3 and Figure 2.1.4. The difference between the simple 1D model results for the temperature and the 2D ANSYS results stem from the size of the cooling holes. The 1D model has been set up for narrow and long holes (such as in the disks of Figure 2.1.1) and therefore underestimates the heat generation in the tangential direction between the holes. The von Mises stress result is typical for Bitter disks: the stress is high on the inner radius and decays with a 1/*r* dependence towards the outside of the disk. The cooling

This project has received funding from the European Union's Horizon 2020 research and innovation programme under Grant Agreement No 871106

holes disrupt the tangential flow of electrical current, expelling current from the area between the holes, leading to a peak in the current density at the sides facing the inner and outer radius of the disk. This peak in current density causes a peak in the von Mises stress at the same location (gray areas in Figure 2.1.4). The expelling of current in between the cooling holes explains the lower stress (green/blue colors) in those areas. As the gray areas (high stress) are small and comparable to results for working Bitter disks, we expect little problems because of this. Should a crack in the material appear here, and start to grow in the radial direction, then this will have a serious effect on the current running through the disk, which easily translates into a detectable voltage change. Coil protection systems can detect such a voltage and intervene before the crack leads to serious issues in the entire coil.

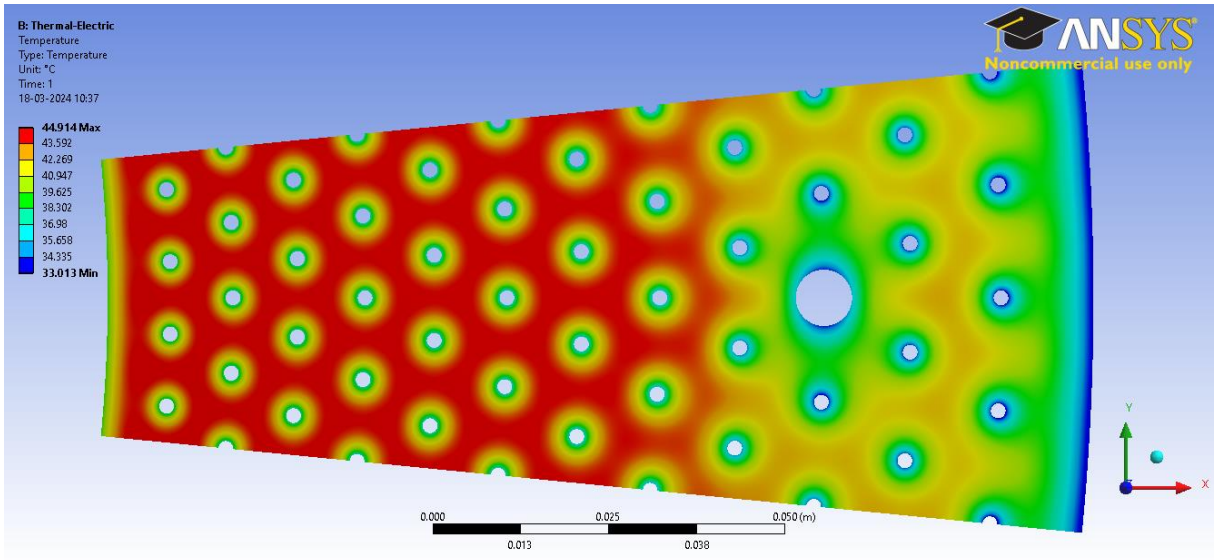

Figure 2.1.3: New inner Bitter coil (HFML model) temperature distribution in the midplane for I = 31 kA. The maximum temperature is about 45°C.

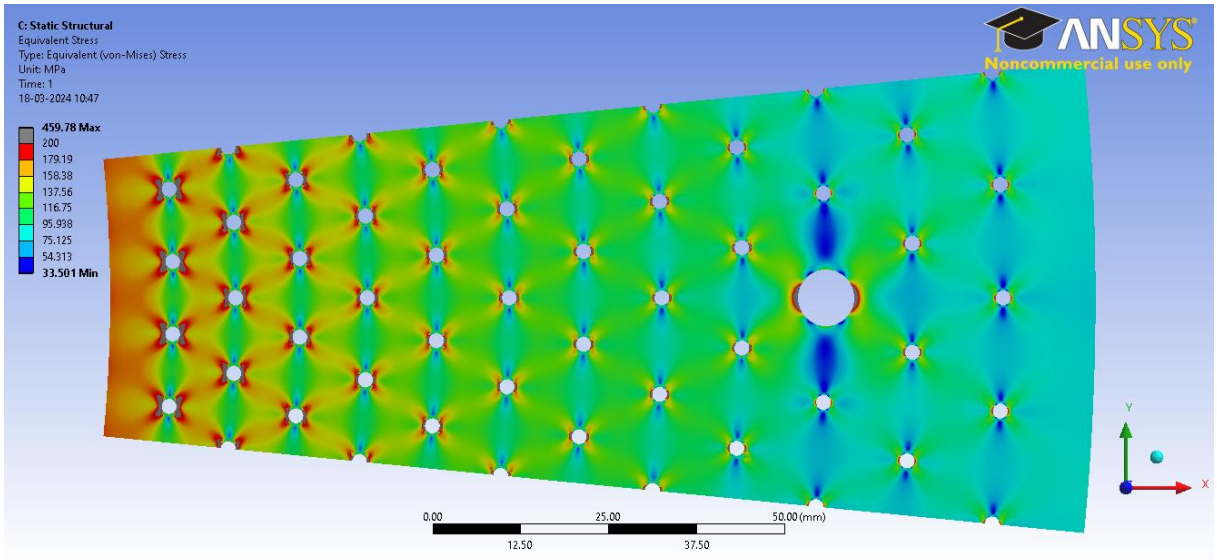

Figure 2.1.4: New inner Bitter coil (HFML model) von Mises stress distribution in the midplane. The maximum von Mises stress in the new configuration is about 250 MPa compared to 225 MPa in the previous design.

This project has received funding from the European Union's Horizon 2020 research and innovation programme under Grant Agreement No 871106

Further comparisons were performed between the new 2D/Axi model and the 2D calculations in the midplane. It shows that our 2D/Axi model gives fair estimates of the temperature and the stress level. However, the 2D/Axi model does not give an "average" temperature profile nor an average stress profile when comparing the solutions at z = 0. This is linked to our cooling models' assumptions, which is not adapted to the shape of the cooling holes considered here. Benchmarks, with elongated cooling slits, show that the discrepancy between the 2D/Axi model and 2D results at z = 0 reduces as the "filling factor" – aka the ration between actual cooling-slits wetted perimeter and modelled cooling rings – tends to 1.

2.1.3 Redesign of the inner magnet

With the above-described common basis and understanding of the design models used in both labs, we investigated a new design for Bitter magnets that are in operation at the LNMCI. The magnets consist of a pair of large diameter Bitter coils providing a background field of around 10 tesla in a free bore of 376 mm in diameter. A set of poly-helices - a magnet technology specific to LNCMI, is operated inside these Bitter coils, to reach a maximal field intensity of 37 tesla. The Bitter coils are derived from a technology introduced by Francis Bitter in the 1930s at MIT. Their design dates from 1999 and is adapted for an available power of 12.5 MW.

A power installation upgrade at the Grenoble facility is ongoing (from 24.5 MW to 30 MW). Starting from 2024 a maximum of 18 MW DC Power will be available to power the Bitter coils. About 10 years ago, similar large diameter Bitter coils were designed at the High Field Magnet Laboratory (HFML), the Dutch magnetic field facility in Nijmegen. The European Magnetic Field Laboratory (EMFL), therefore, has two "in house" designs of large-diameter Bitter coils.

We carried out a design study to investigate the possibilities that both coil sets will be suitable for the available extra power. We explored both practical solutions with existing Bitter disks and optimized solutions with new disks.

In a first section, we present the preliminary design that has been defined to prepare Bitter coils for the new 18 MW DC power converter. Then, we explore a more advanced design to see what magnetic field can be reached with the newly 18 MW available.

2.1.4 Preliminary Design

As stated in the introduction, the actual magnet design consists of an insert that is a set of polyhelices inside two Bitter coils powered separately with 12.5 MW each. The characteristics of the Bitter coils are given in Table 2.1.1. Each coil is composed of three sections. The central section, which contributes most to the magnetic field, contains the largest number of turns n. The mean temperature $<T>$, maximum Hoop stress $\bar{\bar{\sigma}}_H$ and dissipated power P are given at nominal current I = 31 kA with a cooling-water flow of 120 l/s and 25 bar. The Hoop stress is computed considering only the magnetic field generated by the Bitter coils.

This project has received funding from the European Union's Horizon 2020 research and innovation programme under Grant Agreement No 871106

r_1 [mm]	r_2 [mm]	L [mm]	n [-]	<T> [°C]	P [MW]	$\bar{\bar{\sigma}}_H$ [MPa]
199	341	152.1	23	27.23	0.83	141.63
		293.7	86	40.73	6.30	220.42
		152.1	23	27.23	0.83	141.63
343	500	91.1	7	28.33	0.18	21.55
		411.2	62	39.96	3.23	76.92
		91.1	7	28.33	0.18	21.35

Table 2.1.1: 12.5 MW Bitter coils with r_1 the inner bore radius, r_2 the outer bore radius, L the length of the stacking. The inlet water temperature is assumed to be about 12°C.

To account for the power upgrade to 18 MW, while keeping the available Bitter disks at our disposal, we simply increase in a first step the size of the central section of the innermost coil. This allows us to quickly get a new stacking scheme and to minimize the impact on the assembly process and the commissioning of the magnet, since these operations are, by nature, rather complex and time consuming.

The 18 MW installation would deliver a nominal current I_o = 33 kA. In this configuration, the outer coil would dissipate 3.97*33/31=4.23 MW. We can expect the inner coil to dissipate P= (18-4.23) MW at most. If we assume that the water cooling allows the temperature in each section to remain almost constant, it follows that the resistance of each Bitter section is constant and depends only on the section length L. As $P= (2R_e+R_c)/I_o^2$, with R_c the resistance of the central section and R_e the resistance of the end section, we can estimate L_e and L_c. The final inner Bitter coil characteristics are given in Table 2.1.2. The total height of the Bitter coil has slightly changed from the original version to account for the new stacking after assembly.

r_1 [mm]	r_2 [mm]	L [mm]	n [-]	<T> [°C]	P [MW]	$\bar{\bar{\sigma}}_H$ [MPa]
199	341	38.9	6	31.22	0.23	98
		522.6	158	44.13	13.51	277.66
		38.9	6	31.22	0.23	98

Table 2.1.2: 18 MW Inner Bitter.

Shortly after completion of this design, there was an opportunity at the LNCMI - after the failure of the existing coils after more than 5,000 hours of operations - to implement this new design, when the inner Bitter coil needed to be restacked. Our pre-design was promoted using the methods described in the first section of this report to an actual design and used for the new coil. When this coil was tested, we found that the new Bitter magnets produced 12.21 tesla at 16.9 MW and I = 32.5 kA. The 2D Axi model gives the following estimates for this new configuration: 12.14 tesla for 17.9 MW. These estimates are better than the ones from the design since we use a more adapted model for the cooling. Figure 2.1.5 shows the good agreement between measurements and calculations (2D Axi). The estimated values are better for the outer Bitter coil than for the inner one. Our model gives conservative values for the voltage drop on the inner Bitter coil. However, as stated in the previous section, the 2D Axi cooling model is somehow too simplistic. To improve our model, we would need either to

This project has received funding from the European Union's Horizon 2020 research and innovation programme under Grant Agreement No 871106

rework the 2D Axi model with a different approach for the cooling slits or move to a 3D model. Some efforts were done in that direction, but creating a 3D mesh for a complete Bitter coil proved to be difficult. This would also lead to a large model requiring some High Performance Computing resource to run the simulations.

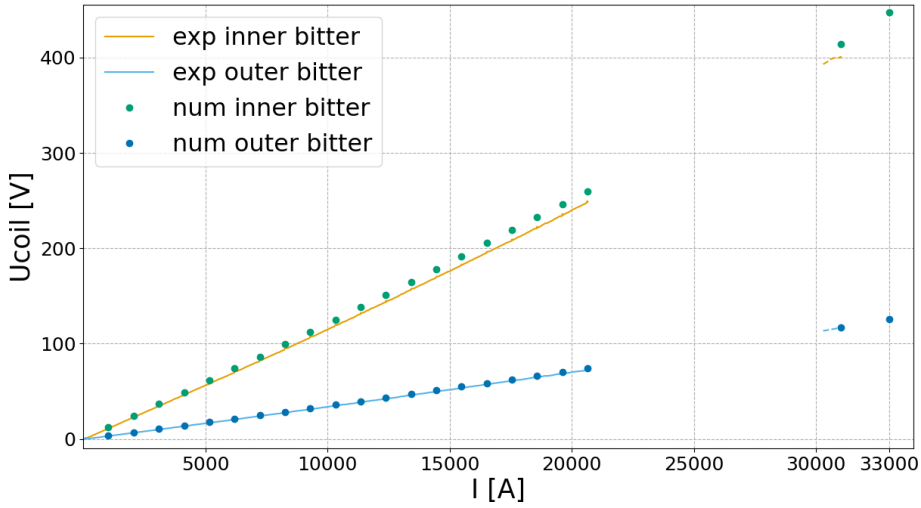

Figure 2.1.5: Comparisons of measured (plain lines) and computed voltage drop (dots) for the inner and outer Bitter.

2.1.5 Redesign of the outer magnet

In the coil designs described above, we have changed the number of windings in the different coil sections. Obviously, increasing the number windings with a high current density increases the magnetic field generated by the coil. For the inner Bitter coil, it is rather straightforward to do this. For the outer Bitter coil, this is less effective because the current density in those windings is rather low and the bore is large. In the central section of the outer coil, a winding is built with eight Bitter disks as four sets of two disks in parallel. With a disk thickness of 0.8 mm, the windings have a thickness of 6.4 mm, excluding the insulator which is typically 0.15 mm thick. If we want to increase the current density in this coil, we need to decrease the winding thickness. However, using only four disks in a winding increases the current density so much that the hoop stress on the disk exceeds the strength of the material. There are two ways to then increase the winding thickness: either we produce new disks of a different thickness, or we change from a regular stacking to an irregular stacking scheme. The first option is expensive and, therefore, less appealing. The second option is much cheaper; it only requires new insulator parts depending on the choices made. In an irregular stacking scheme, we play with the number of disks in a winding.

For instance, if we use only six disks and not eight in a winding by placing 1-2-1-2 disks in each step of the winding, the multiplicity remains 4. This causes current density variations along the axis of the coil, which leads to inhomogeneities in the magnetic field. This can be used to counter inhomogeneities present in the system, but otherwise it is an effect we do not seek. We can also achieve our goal by changing the multiplicity of the winding that is the number of steps within the winding. An example of this is the regular irregular pattern used in the 38 T magnets at the HFML. In that case, rather than making all steps of equal angular length, for the outer

This project has received funding from the European Union's Horizon 2020 research and innovation programme under Grant Agreement No 871106

Bitter coil here 90°, we make three steps of 90° and one step that is half a step size bigger, so 135°. This reduces the multiplicity from n to an effective multiplicity of $n_{eff} = (n\text{-}1)+(n+1)/(2n+1)$, so from 4 to 3.56, thus increasing the current density by a factor $n/n_{eff} = 1.13$.

This strategy has been used to redesign the outer Bitter magnet with the goal of increasing the current density in this coil as far as stress limitations on the inner and outer coils would allow. We can reduce the number of disks in a winding from 8 to 6, which increases the current density to 54 A/mm^2 at I_o = 33 kA. This increases the field strength of the outer coil to 4.23 T at a power consumption of 7.0 MW. The total magnetic field of the Bitter magnet then reaches 12.7 T at 17.5 MW, which is a gain of one tesla compared to the design with the modified inner Bitter coil and a gain of two tesla compared to the original design.

When we change the number of disks to six in a winding, we also change the size of the insulator in between the disks. The original insulator covered eight tie-rod holes; the new insulator covers only five tie-rod holes. There are, however, 32 tie-rod holes in a disk, which is not a multiple of 5 and, therefore, the following irregular stacking pattern appears, see Figure 2.1.6. In this stacking pattern, even though one uses six disks to stack a winding, electrically there are 6.375 disks in a winding. This is the number that enters our design calculations.

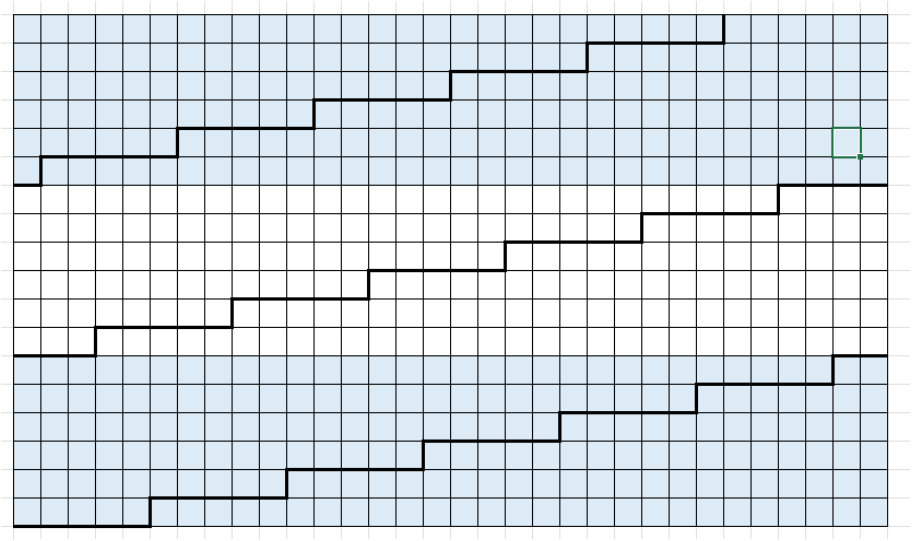

Figure 2.1.6: Irregular stacking pattern for the outer Bitter coil. The rows represent the disks, colors indicate the physical stacking of a winding, i.e. six disks per winding are used. The columns represent the tie-rods, 32 per disk. The thick vertical line is the location of the slit in the Bitter disk and the thick horizontal line is the insulator. In the original stacking, these had a length of eight tie-rods and four insulators were needed to complete a winding. Here we use insulators with a length of five tie-rods, so we need six full pieces and a part (2/5th) of the seventh pieces. Because of this, the slits in the windings do not align at the same tie-rod position, hence the term irregular stacking.

We performed FEM analysis on both temperature and stress for these disks, which shows that there is an issue in cooling this coil. The increased current density at the inner radius leads to a power dissipation that is out of balance with the available cooling. In fact, the temperature in the coil would become unacceptably high, so to make this design work, we need to modify the existing Bitter disks and add an additional ring of cooling holes on the inside. Figure 2.1.7

This project has received funding from the European Union's Horizon 2020 research and innovation programme under Grant Agreement No 871106

shows the temperature analysis of the original disk and the modified disk with the irregular stacking pattern, clearly demonstrating the need for the additional cooling.

This increases the field strength of the outer coil to 4.08 T at a power consumption of 5.9 MW. The total magnetic field of the Bitter magnet then reaches 12.7 T at 17.5 MW, which is a 1.63 tesla gain compared to the original coils.

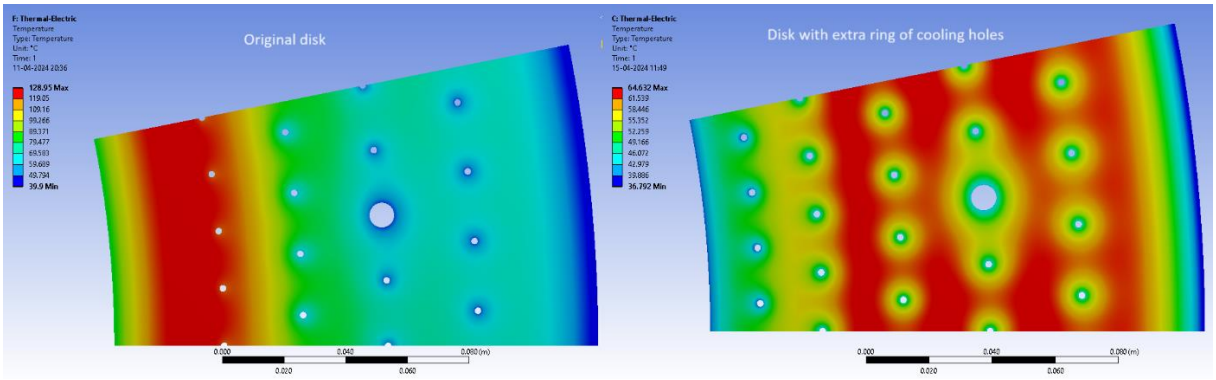

Figure 2.1.7: Comparison of the temperature distribution in the outer disk. On the left hand side, the original disk and on the right hand side the disk with an extra ring of cooling holes.

2.1.6 Conclusions

The Bitter magnet pre-designs for an 18 MW power installation have shown that:

1) Changing the inner Bitter by increasing the high current density section with a regular stacking scheme, 12.32 tesla could be reached at 16.5 MW;

2) Changing the outer Bitter magnet with an irregular stacking scheme provides an additional 0.85 tesla gain to the field.

The inner Bitter magnet has been assembled following the prescribed method after the failure of a 12 MW Bitter magnet at LNCMI. The 1D model used for the pre-design provides some optimistic estimates for the power used. The 2D Axi model gives more precise estimates of the total power with a 6% margin. The difference in the estimation of the total power dissipated is due to the over-estimated voltage drop in the inner Bitter coil. The discrepancy on B at (0,0) is about 0.5% for the magnetic field.

In parallel to the design studies, HMFL and LNCMI have closely worked on the Bitter magnet modelling. Comparisons and benchmarks between their numerical tools have been performed. A newly 2D/Axi FEM have been developed and validated. However, comparisons of the existing and the new models of the 2D Axi results in the Bitter magnet midplane show that the 2D Axi is not accurate enough to give an "averaged" solution of temperature and stress field – especially with the cooling slit shape of the considered Bitter disks. More investigations are needed to improve this model. An alternative would be to consider 3D multi-physics coupled FEM, but creating a mesh for Bitter coils seems difficult. We plan to also put some efforts on this. We estimate that these developments would require 6 months to be fully tested and validated on High Performance Computing ressources.

This project has received funding from the European Union's Horizon 2020 research and innovation programme under Grant Agreement No 871106

The Bitter coils that were investigated in this study are made of almost plain copper. Copper is the best resistive material available. Its conductivity is, by definition, nearly 100% of the international copper standard, so you cannot expect to find better conductors – except by moving towards superconducting materials, but that is outside the scope of the project.

If we apply our new model to more constrained magnets – such as the innermost Bitter magnets from HMFL or the poly-helices insert from LNCMI – the material choice would be more important. However, a compromise between electrical resistivity and material strength has to be considered to keep the material under sustainable stress level while not increasing too much the total dissipated power.

2.1.7 Implementation costs.

Implementation of the first design, with the modified inner Bitter magnet, 'costs' only manpower. The existing and original parts of the coil are reused and restacking a coil typically takes about three weeks with two people for coils of this size.

Implementation of the second design, the modified outer Bitter magnet, will be more costly. Existing parts have to be machined, i.e., adding extra cooling holes in the copper Bitter disks. Depending on the stock of insulating Bitter disk parts, new parts may have to be manufactured. That probably costs 20-30 kEuro, providing the dies for the stamping are still in working condition. The required modifications probably also have a cost in the same range, where material costs could possibly be exchanged for manpower if the modifications can be done by the in-house workshop. Once the parts are available, the stacking work is similar to the period mentioned above.

2.2 Non-destructive pulsed magnets targeting 110 T and beyond at the EMFL

2.2.1 Definition of the electromagnet

This design study has been realized with the objective to make the magnet compatible with both facilities, HLD in Dresden [1] and LNCMI in Toulouse [2], and we decided to impose some constraints to the project. These boundaries are listed below:

- available energy from the existing capacitor banks,
- cryogenics and experimental environment that impose the bore diameter,
- pulses as long as possible to perform actual standard pulsed-field experiments.

First, we will proceed with the optimization of an electromagnet built with existing materials available in sufficient quantities. Then, we consider possible magnet designs with a reduced magnet bore using hypothetical materials, which might be available in the near future. The result of the design study will be the final dimensions of the electromagnet (diameter, length, conducting wire material and cross-section). Some improvements, linked with ongoing research on new materials, will be explored.

Based on the state of the art, designing a triple-coil magnet seems to be the best way to combine an optimal use of available energy and materials in a pulsed magnet system [3]. The three coils (Figure 2.2.1) will be based on an optimized reinforcement density technique [4]. This design study will thus focus on a triple coil and we will explore space parameters to obtain the optimal design before proceeding to finite element analysis.

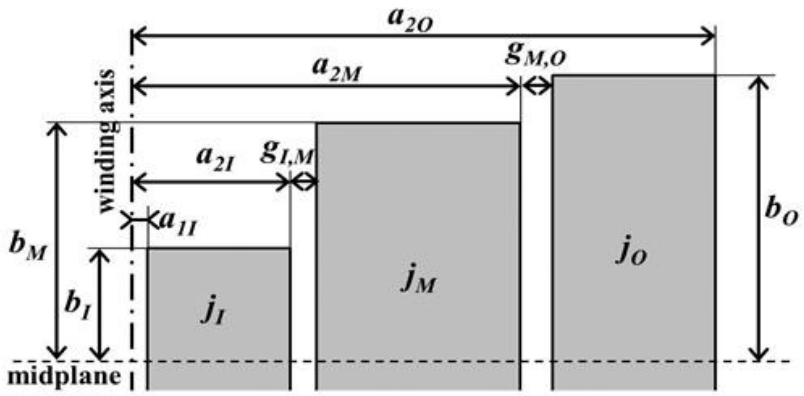

Figure 2.2.1: Scheme of the triple-coil system. I, M, O are for inner, middle and outer coil. j is the current density. a1, a2 and b are inner radius, outer radius and half height, respectively. $g_{I,M}$ and $g_{M,O}$ are the gaps between consecutive coils including a steel cylinder containing the inside coil, a glass fabric/epoxy tube protecting the outside coil bore and space to let liquid nitrogen flow for cooling between the pulses.

The energy for this magnet will be limited by the maximum energy available at LNCMI-Toulouse, where the capacitor banks are smaller than at the HLD.

This project has received funding from the European Union's Horizon 2020 research and innovation programme under Grant Agreement No 871106

Pulse durations for each coil must be at least 3 times longer than the short circuit duration to transfer enough energy from the capacitor bank to the coil. The table 2.2.1 summarizes some important values.

Coil	Maximum energy in capacitor banks (MJ)	Capacitance (mF)	Short circuit rising time (ms)	Short circuit current (kA)	Minimum pulse rising time (ms)
Inner (*I*)	1	3.5	3	36	9
Middle (*M*)	6	20	5	150	20
Outer (*O*)	21	75	21	100	100

Table 2.2.1: Capacitor banks electrical values planned to be used in the design study.

2.2.2 Optimization process

Some dimensions for the coils have to be fixed prior to the optimization process. For example, the bore diameter is chosen to fit standard dimensions for cryogenic equipment such as a helium cryostat. Based on the analytical approach described in the earlier report [5] and the parameters listed in Table 2.2.2, some properties and rough dimensions of the electromagnets can be obtained.

Inner coil		
Conductor ultimate tensile strength	> 1200 MPa	For example Cu-Nb conductor
Conductor electrical conductivity @ 300 K	> 80% IACS	
Conductor electrical conductivity @ 77 K	> 300% IACS	
Magnetic energy	< 750 kJ	Based on the short circuit duration
$2a_{II}$ (Bore diameter)	10 mm	He4 and He3 cryostats available [300 mK < T < 300 K]
Middle coil		
Conductor ultimate tensile strength	> 600 MPa	For example Glidcop
Conductor electrical conductivity @ 300 K	> 90% IACS	
Conductor electrical conductivity @ 77 K	> 400% IACS	
Magnetic energy	< 4.8 MJ	Based on the minimum pulse length
Outer coil		
Conductor ultimate tensile strength	> 450 MPa	For example CuAg0.08%
Conductor electrical conductivity @ 300 K	> 95% IACS	
Conductor electrical conductivity @ 77 K	> 600% IACS	
Magnetic energy	< 17 MJ	Based on the minimum pulse length
κ (Aspect ratio outer diameter/length)	1.675	Optimal value for a single coil
Amount of reinforcement (Zylon fibers)	<25%	A standard value for pulsed magnets of this size

Table 2.2.2: Parameters introduced in the analytical analysis.

To be able to push the magnetic field well beyond the actual limit, it is necessary to decrease the safety margin on the outer coil. As presented in Figure 2.2.2(a), due to the strong inductive

coupling between the coils, the outer coil contributes to the magnet peak field with only 60% of its maximum field. The gain on the outer coil will be around 4 T at the price of a reduced lifetime in case of the non-triggering of the intermediate coil. The calculated von Mises stress distribution in the outer coil is shown in Figure 2.2.2(b).

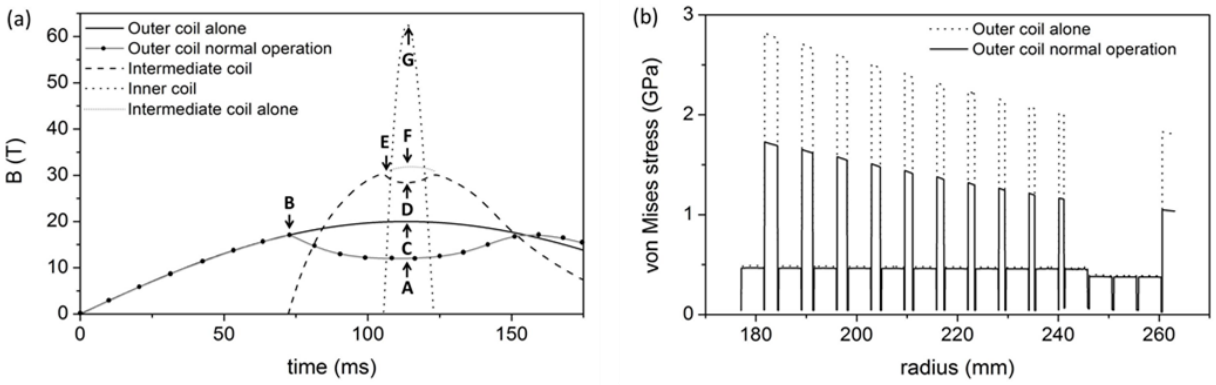

*Figure 2.2.2: (a) Simulation of the magnetic field temporal profile in a triple coil extracted from ref [3]. The magnetic field is considered at the center of the bore and derived from the simulation of the current flowing in the coils. Capital letters on the graph indicate specific magnetic-fields values. The outer coil, when operated alone, reaches 20 T (**C**). Due to a strong inductive coupling with the middle coil, the outer coil only contributes 12 T (**A**) to the total field and reaches 17 T (**B**) just before the triggering of the middle coil. (b) von Mises stress in the outer coil as a function of radius. Dashed lines present the stress in the magnet generating 20 T (**C**). The solid lines show the stress at 17 T, the maximum field reached in normal operation (**B**). In the present design study the **C** point is considered as highly improbable and the magnet will be designed to generate field level **B**. Combined with an increase of the energy of about 50%, it will push the field at the **A** position by about 30%.*

2.2.3 Possible design

Once the dimensions of the system are defined it is possible to elaborate more details for each coil. A summary of the coil properties are listed in Table 2.2.3. For each coil, its contribution to the maximum field is presented in bold. The maximum field generated by the coil during the pulse is described in Figure 2.2.2(a).

Inner coil	**60 T** *(60 T)*	
$2a_{2I}$ (outer diameter)	150 mm	
$2b_I$ (length of the coil)	150 mm	$\kappa = 1$
Conductor cross section	7.4 mm²	copper-stainless-steel composite
Conductor electrical conductivity @ 77 K	180 MS	40% of copper in the cross-section
Conductor + reinforcement filling factor	80%	Remaining 20 % includes wire insulation
Amount of reinforcement (Zylon fibers)	50%	Based on state of the art coils, this is the maximum reasonable quantity
Middle coil	**34 T** *(34.8 T)*	
$2a_{1M}$	170 mm	10 mm gap for coil support and liquid nitrogen flowing
$2a_{2M}$ (outer diameter)	330 mm	
$2b_M$ (length of the coil)	230 mm	$\kappa = 1.43$
Conductor cross section	18 mm²	
Conductor ultimate tensile strength	950 MPa	Copper-stainless-steel composite

Conductor electrical conductivity @ 77 K	235 MS	50% of copper in the cross-section
Conductor + reinforcement filling factor	85%	
Amount of reinforcement (Zylon fibers)	35%	A standard value for pulsed magnet of this size
Outer coil	**16 T** *(22 T)*	
$2a_{1O}$	350 mm	10 mm gap for coil support and liquid nitrogen flowing
$2a_{2O}$ (outer diameter)	490 mm	
$2b_O$ (length of the coil)	280 mm	$\kappa = 1.75$
Conductor cross section	23 mm²	
Conductor ultimate tensile strength	650 MPa	Glidcop AL-60
Conductor electrical conductivity @ 77 K	285 MS	
Conductor + reinforcement filling factor	85%	
Amount of reinforcement (Zylon fibers)	25%	A standard value for pulsed magnet of this size

Table 2.2.3: Coil properties and magnetic-field contribution to the peak field obtained from the optimization process. For the two innermost coils, Copper-stainless-steel macrocomposite conductor [6] has been chosen. It is not commercially available but it offers the best performances at the time of writing the report.

These parameters are used to design a finite elements model using the COMSOL software. The magnetic field map, shown in figure 2.2.3, is used to calculate the electrical properties of the coils summarized in table 2.2.4 and the mechanical stress shown in figure 2.2.4.

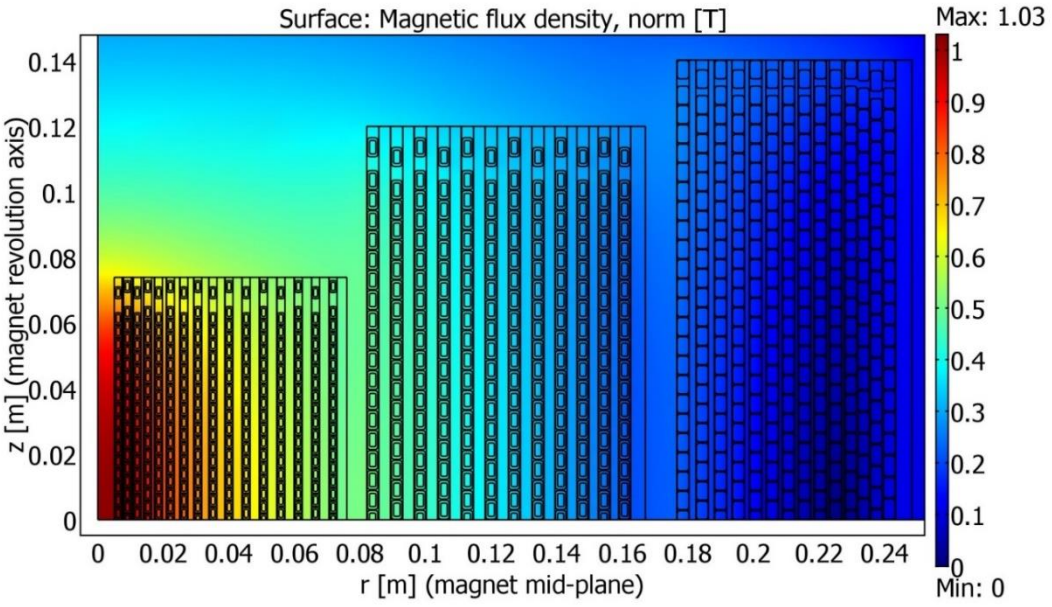

Figure 2.2.3: Magnetic field generated by the triple coil system normalized by the maximum field.

Inner coil	**59 T**
Inductance	4.9 mH
Resistance @ 300 K	710 mΩ
Resistance @ 77 K	99 mΩ
Efficiency I/B	224 A/T
Number of layers	16
Number of turns per layer	34
Length of conductor	122 m
Mass of conductor	7.7 kg
Middle coil	**31 T**
Inductance	25.8 mH
Resistance @ 300 K	750 mΩ
Resistance @ 77 K	100 mΩ
Efficiency I/B	597 A/T
Number of layers	12
Number of turns per layer	36
Length of conductor	340 m
Mass of conductor	53 kg
Outer coil	**20 T**
Inductance	138 mH
Resistance @ 300 K	765mΩ
Resistance @ 77 K	157 mΩ
Efficiency I/B	616 A/T
Number of layers	14
Number of turns per layer	46
Length of conductor	880 m
Mass of conductor	152 kg

Table 2.2.4: Coil properties extracted from the finite elements modeling.

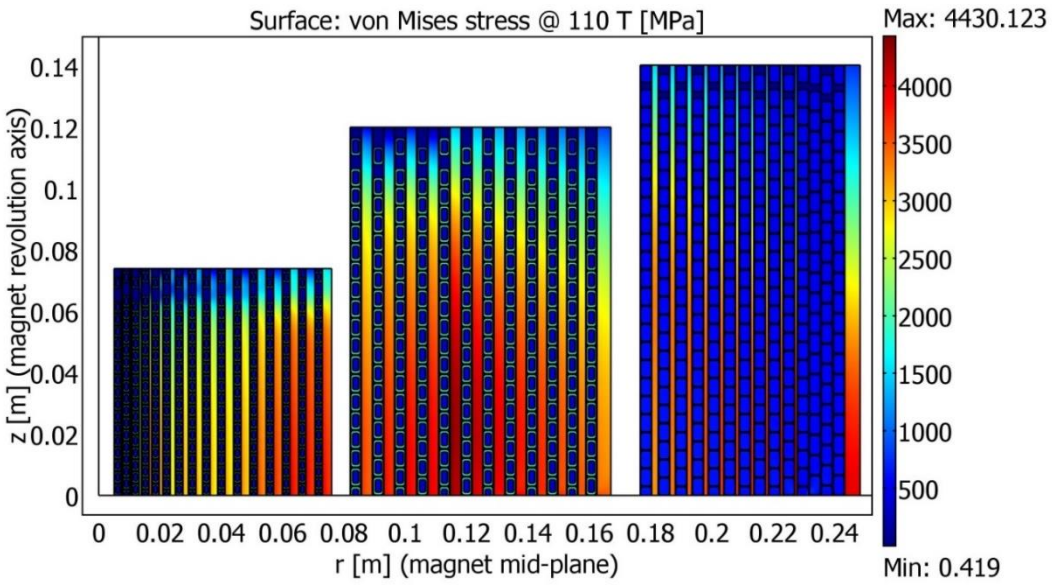

Figure 2.2.4: von Mises stress in the "110 T magnet".

Here, we describe a few options to increase the peak field in the triple-coil magnet.

1) First of all, it is possible to decrease the magnet-bore diameter, resulting in an increase of the magnetic field. However, the small bore diameter would not accommodate most of the existing cryostats and sample holders for various experimental techniques. In this case, a new sample environment should be developed. Another drawback is the challenge to wind the high-strength wires on a small diameter by the magnet manufacturer.
2) Because most of the pulsed magnets are stress limited, another possibility would be to develop new materials with higher ultimate-tensile strength (UTS) of high-conductive wires and reinforcement materials. Such approach demands further intensive research and development efforts. There are already some preliminary promising results for laboratory-scale samples. However, material availability in the quantities required for the magnet production is still due.

Here, using the parameters of the HLD energy supply, we consider how the magnet-bore-diameter reduction can increase the peak field beyond 100 T.

We start with a 100 T design of a triple-coil magnet. Using the following parameters of the magnet and energy supplies (Table 2.2.5), we can obtain magnetic fields of 100 T (Figure 2.2.5).

Coil	Energy (MJ)	Magnetic field (T)	Inner bore (mm)	Length (mm)	Outer diameter (mm)	Wire (mm^2)	Number of layers
Inner coil	1	52	12	130		CuNb 4x6	4
Middle coil	8	35	140	230		Cu 4x6	8
Outer coil	18	13	400	310	600	Cu 4x6	10

Table 2.2.5: Some properties of the HLD 100 T magnet, which serve as a variation on the starting point of the present design study.

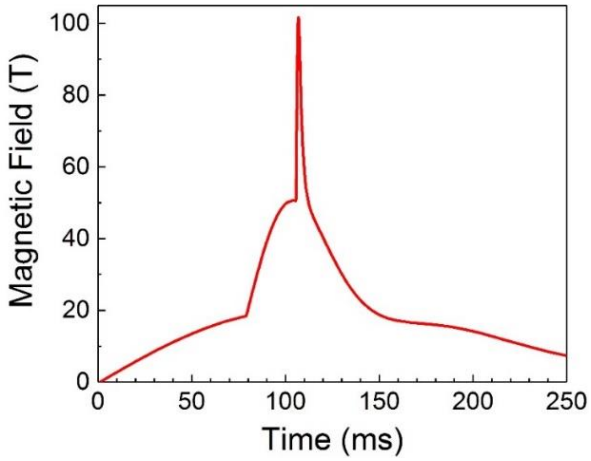

Figure 2.2.5. Calculated magnetic field in a 12 mm bore of the triple-coil magnet.

By optimizing the thickness of the internal Zylon reinforcement, we obtain a maximum of the von Mises stress of 3.3 GPa (Figure 2.2.6) in the internal Zylon reinforcement.

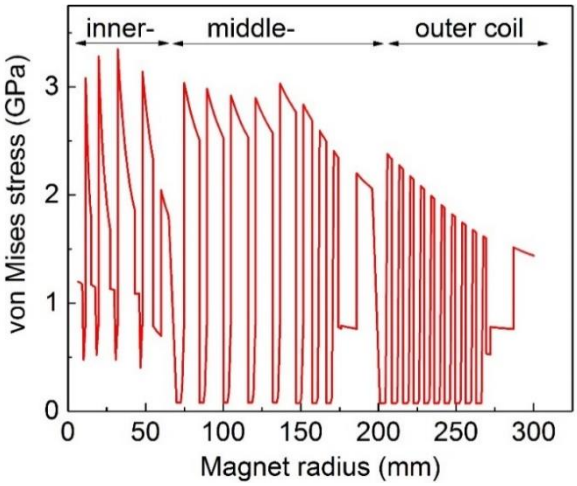

Figure 2.2.6. Von Mises stress at 100 T in the midplane of the triple-coil magnet.

By reducing the bore diameter from 12 to 8 mm and decreasing slightly the resistance of the cables between the capacitor bank and the magnet (this can be done), we obtain ~ 110 T (Figure 2.2.7) at the price of a significantly increased von Mises stress (up to 3.75 GPa, Figure 2.2.8). Obviously, stronger hypothetical materials (for instance, reinforcement fibers with UTS > 5.8 GPa) would level out (or even significantly reduce) the von Mises stress in the magnet.

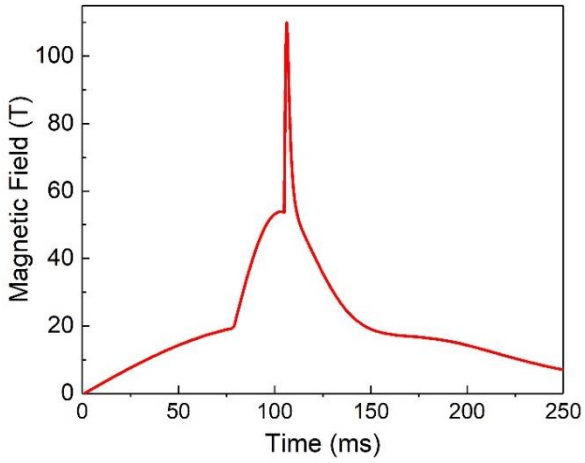

Figure 2.2.7. Calculated magnetic field in 8 mm bore of the triple-coil magnet with other parameters taken from Table 2.2.5.

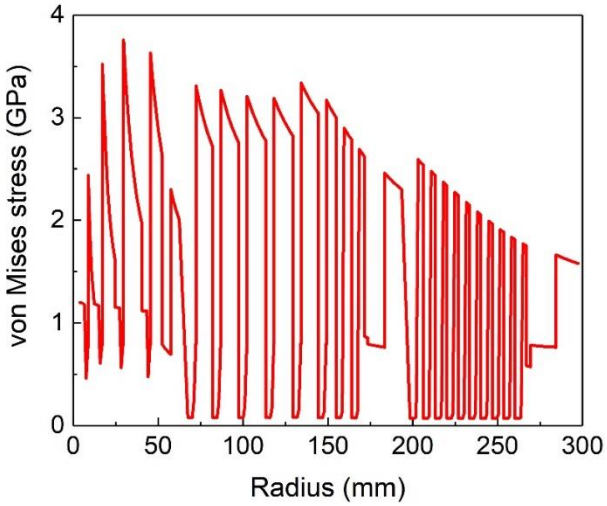

Figure 2.2.8. Von Mises stress at 110 T in the midplane of the triple-coil magnet.

2.2.4 Conclusion and perspectives

The results of this design study show that a triple-coil magnet reaching a peak field of 110 T could be feasible.

Very high pulsed magnetic fields require the use of high performance conductive wires (i.e. exceptional mechanical and electrical properties). Copper-niobium composite, the only commercial wire able to meet this request is produced by a single Russian manufacturer. In the context of the war in Ukraine, this material is no longer available. Solutions are available to replace this conductor by copper-stainless-steel composite produced at LNCMI and used in magnets up to 98.8 T. This conductor as well as the CuNb wire are used in the present design study, but ongoing research and developments on others high strength/high electrical conductivity materials for pulsed magnets are very promising.

Copper and silver composite conductors are developed to go beyond the performance of copper-niobium or copper-stainless-steel. Ultimate tensile strength above 1200 MPa and an electrical resistivity of about 4.6 nΩ.m at 77 K are reached on samples prepared by spark plasma sintering or cold spray [7]. Transferring these developments to industrial scale, or at least to meet the requirements of large coils, is challenging. First scaled-up Ag-Cu wires show that the properties of the wires are not impacted by the upscale, confirming that Ag-Cu composite wire is a very good candidate to replace the Cu-Nb or Cu-stainless-steel wire in inner coils with a possible increase of the maximum field.

Therefore, the availability of high-strength, high-conductivity wires and high-strength reinforcing materials beyond the state of the art would greatly facilitate the design of pulsed magnets operating in the 110 T range.

Other issues to be addressed are the manpower required for the detailed magnet design (estimated to 1 person year, ~100 k€) and the magnet material and construction costs. For instance, at current prices, the conductors and other materials for a 110 T pulsed magnet would cost about 100 k€. The dewar to keep the magnet cold costs approximately 40 k€. In the case

This project has received funding from the European Union's Horizon 2020 research and innovation programme under Grant Agreement No 871106

of in-house production of copper-stainless-steel wire, additional manpower and equipment are required. In this way, the total cost of the 110 T pulse magnet is 400-600 k€ with a total design and construction time of 2 to 3 years.

A magnet using even more energy could be developed and used at the HLD. However, the energy increase results in only a small field gain at the expense of an impractically large and expensive magnet.

2.2.5 References

[1] https://www.hzdr.de/hld.

[2] F. Debray, P. Frings, "State of the art and developments of high field magnets at the Laboratoire National des Champs Magnétiques Intenses", Comptes Rendus Physique, vol. 14, Issue 1, 2013, pp. 2-14, ISSN 1631-0705.

[3] J. Béard *et al.*, "Design and Tests of the 100-T Triple Coil at LNCMI," in IEEE Transactions on Applied Superconductivity, vol. 28, no. 3, pp. 1-5, April 2018, Art no. 4300305, doi: 10.1109/TASC.2017.2779817.

[4] L. Van Bockstal, G. Heremans, F. Herlach, "Pulsed magnetic fields in the 50–70 tesla range with layer by layer reinforced copper coils," Meas. Sci. Technol., pp. 1159–1164, 1991.

[5] Isabel Task 9.4 MAGNET DESIGN CENTER REPORT, November 2023.

[6] F. Dupouy, S. Askénazy, J. P. Peyrade, and D. Legat, "Composite conductors for high pulsed magnetic fields," Physica B, vol. 211, p. 43, 1995.

[7] Simon Tardieu *et al.*, Scale-Up of Silver–Copper Composite Wires by Spark Plasma Sintering and Room Temperature Wire-Drawing for Use in 100 T Triple Coil at LNCMI, IEEE Transactions on Applied Superconductivity PP(99):1-4; August 2024, DOI: 10.1109/TASC.2024.3369011.